Microbial Biotechnology

WILEY

MICROBIAL BIOTECHNOLOGY Open Access

RESEARCH ARTICLE OPEN ACCESS

Immunoassay Detection of SARS-CoV-2 Using Monoclonal Antibody Binding to Viral Nucleocapsid Protein

Robert M. Hnasko[1] | Alice V. Lin[1] | Jeffery A. McGarvey[2] | Eric S. Jackson[2]

[1]United States Department of Agriculture, Agricultural Research Service, Produce Safety and Microbiology Unit, Albany, California, USA | [2]United States Department of Agriculture, Agricultural Research Service, Foodborne Toxin Detection and Prevention Unit, Albany, California, USA

Correspondence: Robert M. Hnasko (robert.hnasko@usda.gov)

Received: 9 September 2024 | **Revised:** 7 February 2025 | **Accepted:** 10 February 2025

Funding: This work was supported by U.S. Department of Agriculture, 2030-32000-011-000-D, 2030-32000-011-007-I.

Keywords: coronavirus | diagnostic | ELISA | immunoassay | lateral flow immunoassay | monoclonal antibodies | nucleocapsid protein | SARS-CoV-2

ABSTRACT

Immunoassays represent sensitive, easy-to-use, and cost-effective tests useful for the detection of the SARS-CoV-2 virus. In this manuscript, we report on the binding specificity of a pair of novel monoclonal antibodies (MAbs) generated against the SARS-CoV-2 nucleocapsid protein (NP) and their development into sensitive sandwich enzyme-linked immunosorbent assays (sELISA) and a lateral flow immunoassay (LFIA). Binding of these MAbs to hCoVs is limited to variants of SARS-CoV-2 and SARS-CoV NP. Chemiluminescent and absorbance spectroscopy sELISAs report a limit of detection (LOD) for the SARS-CoV-2 B.1.1.529 NP variant at 15 pg/mL, and the LFIA using a red-dyed 200 nm particle at 10 ng/mL. The sELISA exhibits broad SARS-CoV-2 viral variant detection with assay LOD for SARS-CoV-2 B.1.1.529 virus at 1.4×10^5 genome copies per mL ($p \leq 0.001$). The availability of these MAbs should facilitate continued investment in the commercial development of immunoassays to increase global SARS-CoV-2 detection technologies.

1 | Introduction

Coronaviruses (CoVs) are enveloped positive-sense RNA viruses that share similarities in their genomic organisation and structural composition (Masters 2006). These viruses are responsible for a variety of pathological conditions in domestic animals and humans (hCoV) that involve infections of the upper respiratory or gastrointestinal tract (Corman et al. 2018). Normally, hCoV infection presents mild, self-limiting disease; but beginning in 2002 with the zoonotic spillover of SARS-CoV (Severe Acute Respiratory Syndrome) and MERS (Middle East Respiratory Syndrome) in 2012, these pathogens resulted in increased disease severity and mortality (Tang et al. 2022). Although the origin of SARS-CoV-2 from Wuhan, China, in 2019 remains enigmatic (Holmes et al. 2021; Alwine et al. 2023), its emergence as hCoV-19 resulted in a global pandemic with enormous societal, economic and human cost (Richards et al. 2022; Blazquez-Fernandez et al. 2023).

Emerging and re-emerging pathogens represent a global challenge for public health (Gostin and Gronvall 2023). CoVs represent prevalent and broadly distributed pathogens that frequently recombine their large genetically diverse genomes, enabling novel virus formation (Masters et al. 2006). Loss of biodiversity, human habitat encroachment, animal husbandry practices, and human-animal cohabitation increase the risk of cross-species infections and zoonotic spillover events (Brown 2004; Sanchez et al. 2021). SARS-CoV-2 remains a highly relevant and dangerous pathogen that continues to propagate and evolve in animal reservoirs with the potential to re-emerge with serious consequences. Moreover, efforts to manipulate such viruses using widely available molecular technologies present new challenges

aimed at limiting future cross-over events either by accident or nefarious action (Yount et al. 2000, 2003; Scobey et al. 2013; Zeng et al. 2016; Berche 2023).

Detection technologies that identify disease-causing pathogens in the environment, or animals and their by-products, remain an essential tool in understanding their distribution and spread, serving a critical part of containment strategies (Chen et al. 2021). The broad penetrance of the SARS-CoV-2 virus in animal reservoirs necessitates effective detection methods for global monitoring of its distribution, transmission, and containment (Prince et al. 2021; Tan et al. 2022). Immunoassays provide sensitive, inexpensive, and simple-to-use tools for the effective detection of the SARS-CoV-2 virus (Alhamid et al. 2022). In this manuscript, we report on the development of novel monoclonal antibodies (MAbs) against the SARS-CoV-2 nucleocapsid protein (NP) and their development into sensitive and selective microplate enzyme-linked immunoassays (ELISA) and lateral flow immunoassay (LFIA) test strips. The SARS-Cov-2 NP is abundant, highly conserved and evolutionarily stable, providing a useful antigenic target for the construction of tests aimed at broad detection of SARS-CoV-2 viral variants (Cubuk et al. 2021; Li et al. 2022; Song et al. 2023). Continued development of these molecular tools serves to de-risk critical technology that facilitates and promotes commercial investment to increase the global availability of inexpensive tests for widespread SARS-CoV-2 detection applications.

2 | Material and Methods

2.1 | Hybridoma Technology

All chemical reagents were of the highest grade commercially available. Female Balb/cByJ mice (The Jackson Laboratory, ME) at 6 weeks of age were immunised every 10d, 4 times, by intraperitoneal inoculation with a 50 μL emulsion of 5 μg recombinant SARS-CoV-2 nucleocapsid protein (NP) Omicron B.1.1.529 variant from human embryonic kidney (HEK) cells (Acro Biosystems, DE) diluted in equal volume in TiterMax gold adjuvant (Sigma, MO). Briefly, harvested splenocytes were chemically fused using dilute stepwise poly(ethylene glycol) of 3000–3700 molecular weight (Sigma) with a nucleotide salvage pathway deficient, aminopterin sensitive, SP2/0 myeloma cell line to generate hybrid cells (Hnasko and Stanker 2015). Fused cells were incubated in tissue culture flasks at 37°C with 5% carbon dioxide in Iscove's media containing 10% fetal bovine serum (FBS) and HAT (hypoxanthine-aminopterin-thymidine). After 3d, viable cells were collected after centrifugation on Histopaque-1077 (Sigma) and plated in 96-well tissue culture microplates. After 10d high-throughput screening and selection of anti-SARS-CoV-2 monoclonal antibody (MAb) producing hybridoma cells were performed using cell conditioned media (CM) from 96-well microplates by indirect and capture enzyme-linked immunosorbent assay (iELISA and cELISA) methodologies (see below) using recombinant SARS-CoV-2 NP Omicron variant B.1.1.529 derived from *Escherichia coli* (Sino Biological, TX). Hybrid cells selected for SARS-CoV-2 NP MAb production were cloned by limiting dilution in Isocove's media containing 10% FBS and HT (hypoxanthine and thymidine), expanded into cell lines and CM harvested for MAb purification by Protein-G affinity chromatography (HiTrap; Cytiva, MA) (Hnasko and McGarvey 2015). A cohort of hybridoma cell lines producing MAb against SARS-CoV-2 NP were evaluated for pairwise performance in a sandwich ELISA (sELISA) format with the best MAb pair selected for assay construction and optimization (see Table S1). The hybridoma cell line producing MAb 4D4 (IgG1, kappa) was selected for immobilisation and 1H6 (IgG1, lamda) selected for reporter functionalization (Hnasko 2015a).

2.2 | Western Blotting

Recombinant human coronavirus nucleocapsid protein (hCoV NP) (see Table 1) concentrations were verified by spectroscopy (Nanophotometer N50, Implen, CA) and normalised in LDS buffer (lithium dodecyl sulfate, glycerol, Coomassie G250 and Phenol Red, pH 8.4) containing the reducing agent TCEP (tris(2-carboxyethyl)phosphine) at 50 mM, then heat denatured for 10 min by boiling. Electrophoresis of 1 μg of protein through 4%–12% BIS-Tris gels (Thermo Fisher Scientific, CA) was used to separate various hCoV NP and a colour protein standard (BioRad, CA) based on charge and molecular weight prior to protein transfer to nitrocellulose membranes. Nitrocellulose membranes were washed in TBST (Tris-buffered saline with 0.1% Tween-20, pH 7.4), blocked in 10% non-fat dry milk (Lab Scientific bioKEMIX Inc., MA) then probed with 4D4 or 1H6 MAb directly conjugated to horse radish peroxidase (Lightning-Link HRP, Novus Biological, CO) followed by chemiluminescent signal generation (Pierce PicoECL; Thermo Fisher Scientific) and detection with image acquisition using a ChemiSOLO instrument (Azure Biosystems, CA) at various times (Hnasko and Hnasko 2015).

2.3 | Enzyme-Linked Immunosorbent Assay (ELISA)

All chemiluminescent ELISA assays were performed on black, flat-bottom, high-binding (HB) 96-well microplates (Fluotrac600; Greiner Bio-One, NC). An antigen-specific HRP-conjugated MAb or molecular reporter was used with an enhanced chemiluminescent substrate (Ultra ECL; Neogen, MI) then analysed using a Victor X3 multimode microplate reader (Perkin-Elmer, CT) and reported in counts per second (CPS). All colorimetric ELISA were performed in clear, flat-bottom, HB-microplates (Strip plate; Greiner Bio-one) with an HRP-reporter conjugate and TMB (3,3′,5,5′-tetramethylbenzidine) substrate (K-Blue Advanced TMB, Neogen). Analysis of the blue reaction product was performed using the Victor X3 (bottom read) and expressed as absorbance at 650 nm. Antigen or antibody immobilisation to HB-microplates was performed in 100 μL of 0.2 M carbonate–bicarbonate buffer (pH 9.4) for 1 h at room temperature (RT). Indirect ELISA (iELISA) was performed during hybridoma screening and selection and used a goat-anti-mouse IgG gamma-chain HRP-conjugate (1:10 K; Sigma-Aldrich) reporter for detection (Hnasko et al. 2011). Capture ELISA (cELISA) were performed during hybridoma selection and characterisation. Antibody immobilisation from CM to the microplate was facilitated using an affinity-purified goat-anti-mouse IgG1-3 Fc gamma-chain specific antibody

TABLE 1 | Origin and details of recombinant viral nucleocapsid proteins (NP) used in experimental data.

#	Nucleocapsid (NP)	Manufacture product #	Recombinant host Predicted MW	NCBI code	NW score	Terminal 6× HIS
1	SARS-CoV-2 (B.1.1.529)	Sino Biological 40588-V07E34	*Escherichia coli* 46 kDa	YP_009724397.2 Variant B.1.1.529	2176	N—
2	SARS-CoV-2 (B.1.1.529)	Acro Bio systems NUN-C52Ht	HEK 293 Cells 55-65 kDa	YP_009724397.2 Variant B.1.1.529	2176	C—
3	SARS-CoV-2 (Wuhan-Hu-1)	East Coast Biologics LA600	*Escherichia coli* 48 kDa	YP_009724397.2	2148	C—
4	SARS-CoV	Sino Biological 40143-V08B	Sf9 Insect Cells (BV) 48 kDa	YP_009825061.1	1973	C—
5	MERS-CoV	Sino Biological 40068-V08B	Sf9 Insect Cells (BV) 47 kDa	AFS88943.1	925	C—
6	hCoV-OC43	East Coast Biologics LA659	*Escherichia coli* 50 kDa	YP_009555245.1	538	C—
7	hCoV-HKU1	East Coast Biologics LA658	*Escherichia coli* 50 kDa	YP_173242.1	546	C—
8	hCoV-NL63	Acro Bio systems NUN-V5146	*Escherichia coli* 50 kDa	YP_003771.1	345	C—
9	hCoV-229E	East Coast Biologics LA638	*Escherichia coli* 47 kDa	NP_073556.1	294	N—

Note: The SARS-CoV-2 NP shares 90.5% identities and 94.3% sequence similarity with SARS-CoV NP (Mohammed 2021). The NW Score is based on Needle-Wunsch algorithm for pairwise sequence alignment to the SARS-CoV-2 B.1.1.529 Omicron variant. Global alignment program Needle (EMBOSS) EMBL-EBI.

(Jackson ImmunoResearch) or after MAb purification by direct absorption (Stanker and Hnasko 2015). Recombinant antigen was biotinylated directly (Lightning-link Rapid Type A; Novus) and detection reported using an avidin-peroxidase conjugate (1:30 K; Sigma-Aldrich). See Table S1. Direct ELISA (dELISA) was performed during MAb characterisation using HRP-MAb conjugates (Lightning-Link HRP; Novus) (Hnasko 2015b). After antibody or antigen immobilisation, wash steps used TBST buffer (200 μL × 3), block was 10% NFDM in TBST (200 μL × 0.5 h RT), sample diluted in TBST (100 μL × overnight RT), HRP-conjugate diluted in TBST (100 μL × 1 h RT) and substrate (100 μL × 2 min RT) (Hnasko et al. 2022). The optimised sandwich ELISA (sELISA) used microplate immobilised 4D4 MAb at 2 μg/mL and 1H6-HRP reporter at 1 μg/mL. Antigens evaluated include recombinant hCoV NP (see Table 1) and heat or gamma irradiated SARS-CoV-2 viral variants samples (see Table 3). All viral samples were obtained through BEI Resources, NIAID, NIH including NR-52287, contributed by the Centers for Disease Control and Prevention, NR-55350; NR-55351; NR-56129, contributed by Andrew S. Pekosz and NR-56496, contributed by Mehul Suthar.

2.4 | Lateral Flow Immunoassay (LFIA)

A BioDot XYZ3060 instrument (BioDot, CA) fitted with a non-contact BioJet valve was used to dispense 40 nL drops at 1 μL/cm for the test line (T), 4D4 MAb at 3 mg/mL, and the control line (C), donkey-anti-mouse-IgG (H + L) at 1 mg/mL (Jackson ImmunoResearch, MA) on Hi-Flow Plus 90 nitrocellulose membrane cards (Millipore, MA). Nitrocellulose membranes were forced air dried at 37°C for 2 h, then blocked in 0.15% poly(vinyl alcohol) molecular weight 9-10 K, 80% hydrolyzed (Millipore) and dried a second time (Ching et al. 2012, 2015; Hnasko et al. 2019, 2021). Briefly, the 1H6 MAb was covalently conjugated to 192 nm, red-dyed, carboxylated polystyrene latex microspheres (Bang labs, IN) using 1-Ethyl-3-(3-dimethylaminopropyl)carbodiimide (EDC) and N-hydroxysulfosuccinimide (Sulf-NHS) chemistry. An AirJet valve on the BioDot XYZ3060 was used to dispense the 1H6 MAb conjugate as a 0.25% solid at a rate of 2.5 μL/cm × 8 (~10 mm depth) on Fusion5 material (Cytiva, MA) that was pre-treated with 10% sucrose containing 0.25% Tween-20 and air dried. The test strips were constructed with the Fusion5 serving as both the sample pad and the conjugate release pad, which was applied conjugate side down and overlapped the HF90 membrane by ~2 mm. CF6 material was used as the absorptive sink at the top of the membrane (~2 mm overlap), test strips cut at 4.5 mm using a guillotine cutter (BioDot), placed in a 2-part plastic cassette with a sample well and test window, and desiccated until use. The LFIA sample running buffer composition was 100 mM phosphate buffer (pH. 7.4), 1% Triton-X100, 1% Tween-20, 1 M sodium chloride, and 0.1% NFDM. Samples of 100 μL were applied to the test strip, and after 10 min, photographed using a cell phone camera under white light or analysed by reflectance (mm/mV) using an ESQuant LR3 instrument (Qiagen Lake Constance GmbH, DE) in triplicate.

2.5 | Statistical Tests

Graphical data is expressed as means ± SEM with no less than three independent samples. ELISA dose–response data were

plotted with regression lines drawn using a dynamic four-parameter logistic curve fit model (4PL) on log-linear or log–log scales. These data were used to calculate EC50 (half maximal concentration) and Hill slope to establish standard curves used in the calculated concentration of SARS-CoV-2 NP from unknown samples. Pairwise comparisons of NP or viral samples were made against an equivalent no-antigen control, uninfected Vero E6, or a MERS-CoV-infected cell control to determine the limit of detection (LOD) for each assay. The Shapiro–Wilk test was used to analyse data for normality, and Brown-Forsythe was used to analyse data for equal variance. Data that passed normality was analysed by either Student's *t*-test, when equal variance was assumed, or Welch's *t*-test, when equal variance was not assumed. Data that did not pass normality was analysed using the non-parametric Mann–Whitney *U*-test. Statistical significance was reported in *p*-values, with probabilities > 95% considered significant. All graphic plotting and statistical analysis were performed using SigmaPlot 15.0 software (Grafiti LLC, CA).

3 | Results

Hybridoma technology resulted in a cohort of novel cell lines making anti-SARS-CoV-2 NP MAbs (Table S1). The biochemical properties of each MAb were evaluated and used to determine the optimal pair for immunoassay construction that would be useful in the detection of the SARS-CoV-2 virus. In this manuscript, we characterise the 4D4 (IgG1, kappa) and 1H6 (IgG1, lamda) MAb and show their binding properties to various human coronavirus nucleocapsid proteins (hCoV NP) (Table 1) by immunoassay. We describe the construction and performance of this MAb pair in sELISA and LFIA formats useful in the sensitive detection of the SARS-CoV-2 virus by binding NP.

A direct ELISA was used to evaluate the binding specificity of the 4D4- and 1H6-HRP MAb conjugates to various hCoV NPs (Figure 1). These MAbs exhibit significant binding to the SARS-CoV-2 and SARS-CoV NP as compared to a no antigen or BSA control ($p \leq 0.001$). We observed no statistical difference in either MAb binding to SARS-CoV-2 NP derived from *E. coli* or HEK cells (data not shown), suggesting MAb binding epitopes are independent of amino acid glycosylation. Moreover, there was no significant binding of either MAb to any of the other hCoV NPs tested with data reported for 1 μg/mL. The 4D4 MAb exhibits reduced binding to the SARS-CoV-2 NP Wuhan Hu-1 variant (26%) and 154-fold reduced binding to the SARS-CoV NP as compared to the SARS-CoV-2 NP Omicron B.1.1.529 variant (Figure 1A). However, 4D4 MAb binding to SARS-CoV NP (10-fold) is statistically significant as compared to no antigen or BSA controls ($p \leq 0.001$). At 500 ng/mL of SARS-CoV NP, we observed no 4D4 MAb binding with detection equivalent to our assay background controls (data not shown). 4D4 MAb binding to the Omicron B.1.1.529 variant was ~2-fold better than the 1H6 MAb. Like the 4D4 MAb, the 1H6 MAb binding to the SARS-CoV-2 Wuhan Hu-1 NP was reduced (25%). However, unlike the 4D4 MAb, there was no statistical difference in 1H6 binding to SARS-CoV NP as compared to SARS-CoV-2 Omicron B.1.1.529 NP (Figure 1B). These individual MAb binding properties can be attributed to novel binding epitopes and structural differences in SARS-CoV-2 NP viral variants.

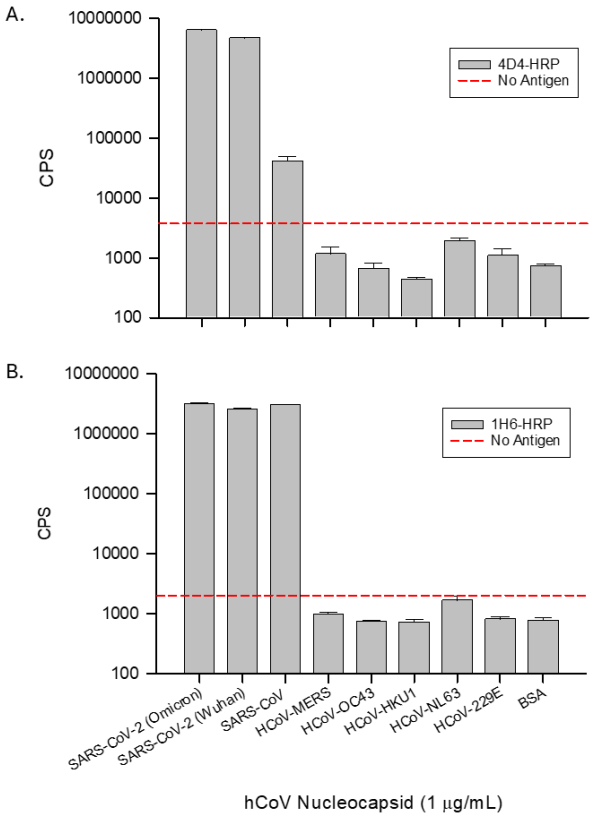

FIGURE 1 | Direct ELISA data reporting the binding of 4D4 (panel A) and 1H6 (panel B) MAbs to hCoV NP. MAbs were conjugated to HRP and binding to 1 μg/mL of recombinant viral nucleocapsid protein (NP) reported with an enhanced chemiluminescent substrate (ECL) and a luminometer. Binding data is expressed as the mean ± SEM in counts per second (CPS) with BSA and no antigen (dashed red line) controls. See recombinant NP details in Table 1 [2–9]. Key: [2] SARS-CoV-2 B.1.1.529 from HEK 293. [3] SARS-CoV-2 Wuhan-Hu-1. [4] SARS-CoV. [5] MERS-CoV. [6] hCoV-OC43. [7] hCoV-HKU1. [8] hCoV-NL63. [9] hCoV-229E.

Western blotting was used to evaluate the binding specificity of the 4D4- and 1H6-HRP MAb conjugates to the hCoV NPs after disulfide reduction and heat denaturation (Figure 2). The hCoV NPs (1 μg) were separated by gel electrophoresis, transferred to nitrocellulose, and blots probed with 4D4 (Figure 2A) and 1H6 (Figure 2B) HRP-MAb conjugates using a chemiluminescent substrate with image acquisition after 30 s. The 4D4 and 1H6 MAb both bind Omicron B.1.1.529 and Wuhan Hu-1 SARS-CoV-2 NP variants at expected molecular weights, with protein migration of Omicron B.1.1.529 NP from HEK cells (55–65 kDa) differing from NP produced in *E. coli* (~46 kDa) as a function of amino acid glycosylation. No binding was detected to the SARS-CoV NP or any of the other hCoV NPs with the 4D4 MAb (Figure 2A). The 1H6 MAb bound the SARS-CoV NP but no other hCoV NP (Figure 2B). No additional bands were observed in either blot after > 5 min exposure, and membrane counterstain (Ponceau S) revealed target protein in all lanes (data not shown). The loss of SARS-CoV detection after heat denaturation with only the 4D4 MAb suggests a NP binding epitope that differs from that used by the 1H6 MAb.

The sandwich ELSIA (sELISA) is an established immunoassay format that provides a simple, sensitive and low-cost method for

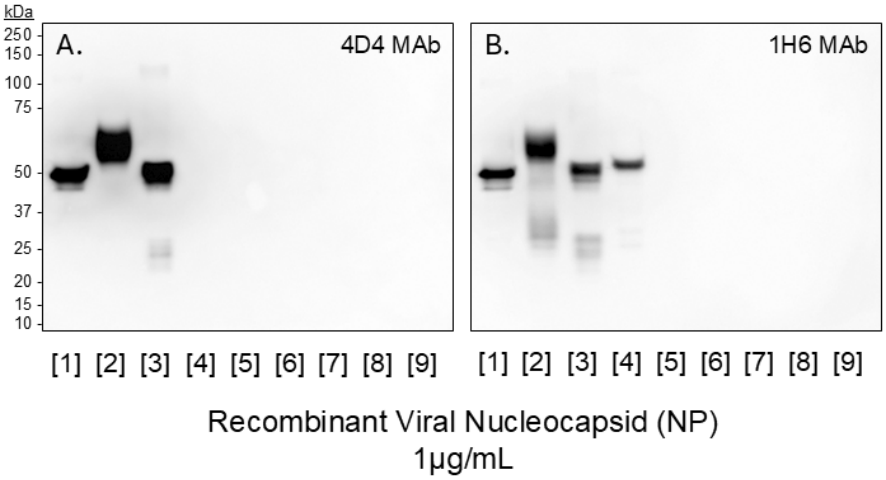

FIGURE 2 | Western blots showing the detection of disulfide reduced and heat denatured recombinant viral nucleocapsid proteins (NP) after electrophoresis (1 µg) with 4D4 (panel A) and 1H6 (panel B) MAb. Images were acquired at 30 s from nitrocellulose blots using a chemiluminescent substrate with HRP-conjugated MAb (1 µg/mL) detection. A mixed standard was used to define protein migration by molecular weight (kDa). See recombinant NP details in Table 1 [1–9]. Key: [1] SARS-CoV-2B 1.1.529 from *E. coli*. [2] SARS-CoV-2 B.1.1.529 from HEK 293. [3] SARS-CoV-2 Wuhan-Hu-1. [4] SARS-CoV. [5] MERS-CoV. [6] hCoV-OC43. [7] hCoV-HKU1. [8] hCoV-NL63. [9] hCoV-229E.

the qualitative or quantitative detection of target antigens (Shen et al. 2014; Sakamoto et al. 2018). It requires a pair of antibodies that function together to bind available antigen epitopes in a liquid sample. One immobilised antibody is used to capture the target analyte, and another antibody, functionalised with a molecular reporter, is used to bind the immobilised antibody–antigen complex for detection. In this manuscript, we report only data on the optimal MAb pair used in the construction of the SARS-CoV-2 NP sELISA after empirical determination by pairwise comparison of MAbs from our established cohort (Table S1). In Figure 3 we report dose–response curves for two sELISAs using immobilised 4D4 and 1H6-HRP MAbs for the detection of the SARS-CoV-2 B.1.1.529 NP. The data plot the mean ± SEM of SARS-CoV-2 NP detection at each concentration, and the solid line represents four-parameter logistic (4PL) curve fit data. Detection for the chemiluminescence sELISA (Figure 3A) was interrogated using a luminometer and expressed in counts per second (CPS). The blue reaction product of the TMB colorimetric sELISA (Figure 3B) was interrogated using absorbance spectroscopy at 650 nm. The EC50 (half maximal effective concentration) of the assay are graphically plotted (vertical dashed lines) and values are reported in Table 2 with the curve Hill Slope and limit of detection (LOD). The LODs of both sELISAs were identical, with sensitivities of 15 pg/mL ($p \leq 0.025$) for SARS-CoV-2 NP. The quantitative range for each assay as standard curve was ~3log order, with an EC50 of 4.15 ng/mL for the chemiluminescent assay and 1.55 ng/mL for the TMB assay with 650 nm absorbance. Antibody self-pairing was effective in the detection of the recombinant SARS-CoV-2 NP, but with diminished sensitivity when compared to the novel MAb pair (data not shown). Antibody self-pairing is consistent with the dimerisation of the NP in solution (Zeng et al. 2020). Reversing the MAb pair orientation, where 1H6 was immobilised and 4D4 functionalised with HRP, was also less sensitive in detection of the NP (data not shown).

To assess the performance of the sELISA for the detection of the SARS-CoV-2 virus, we used irradiated Calu-3 cells passaged hCoV19/USA/GA-EHC-2811C/2021/Omicron B.1.1.529 variant. In Figure 4 we report sELISA detection (mean ± SEM) of serially diluted SARS-CoV-2 infected Calu-3 cell extract and a cell culture media control (2% FBS CM). Detection by chemiluminescent sELISA (Figure 4A) is plotted as log CPS versus the TCID50/mL with a LOD of 37 TCID50/mL or 1.44×10^5 viral genome equivalents per mL ($^*p = 0.022$). The TMB sELISA (Figure 4B) is plotted as linear absorbance at 650 nm versus the TCID50/mL with a LOD (Figure 4C) of 146 TCID50/mL or 5.67×10^5 genome equivalents per mL ($^*p = 0.004$). The TMB substrate results in a visible colour reaction product, and without instrumentation, the SARS-CoV-2 virus is visually reported at 586 TCID50/mL or 2.28×10^6 genome equivalents per mL (Figure 4D).

To further characterise the sensitivity and selectivity of the sELISA, we evaluated four distinct SARS-CoV-2 viral variants passaged in tissue culture and inactivated by heat or gamma irradiation (Table 3). All viral samples were normalised by dilution to 1×10^4 TCID50/mL, then serially diluted further, and viral detection was determined by chemiluminescent sELISA. A MERS-CoV infected and uninfected Vero E6 cell were used as assay controls, and their binding was equivalent to background. At a dilution of 5×10^3 TCID50/mL, all SARS-CoV-2 viral variant samples evaluated ($N = 8$) were statistically significant ($p \leq 0.001$) when compared to either the MERS-CoV infected or Vero E6 controls (Figure 5). The LOD for each viral variant sample was determined from the serial dilution and reported in viral genome equivalents per mL in Table 3. The most sensitive detection was from the gamma irradiated SARS-CoV-2 USA-WA1/2020 variant at 4.3×10^4 genome equivalents per mL ($p = 0.005$), and the least sensitive detection was from the heat denatured hCoV-19/USA/GA-EHC-2811C/2021 variant at 4×10^6 genome equivalents per mL ($p \leq 0.001$).

One of the criteria for the selection of the 4D4 and 1H6 MAb pair was applicability and performance in a LFIA. To construct a LFIA, the 4D4 MAb was immobilised on nitrocellulose membranes and the 1H6 MAb functionalised with a 200 nm red-dyed

particle reporter, allowing visual detection of the SARS-CoV-2 NP or virus on test strips (Figure 6). Photographs of LFIA test strips showing a SARS-CoV-2 Omicron B.1.1.529 NP variant sample dilution series that reports a LOD of 10 ng/mL by visual inspection at the test (T) line (Figure 6A; *left side*). Photographs of a virus positive LFIA test show positive test line detection from irradiated SARS-CoV-2 B.1.1.529 infected Calu-3 cell extract (TCID50/mL = 7.5×10^5) as compared to a corresponding negative control (Figure 6A; *right side*). LFIA test strips from samples run in triplicate were scanned and reflectance peak test line data collected, then plotted as mean ± SEM of the peak area (mm mV) and reported in Figure 6B. Samples containing ≥ 10 ng/mL of SARS-CoV-2 NP or 7.5×10^5 TCID50/mL of virus were significantly different from sample controls ($p = 0.037$ and $p \leq 0.001$, respectively) at the test line. Representative LFIA test strip photographs of 2 μg/mL of various hCoV NP are reported in Figure 6C. A visually positive test line is observed with both the Wuhan Hu-1 and Omicron B.1.1.529 SARS-CoV-2 NP variants, with a faint test line visible for the SARS-CoV NP. No other hCoV NP resulted in a positive LFIA test line (T) at any concentration evaluated, with assay performance for all negative test samples confirmed by positive control (C) lines.

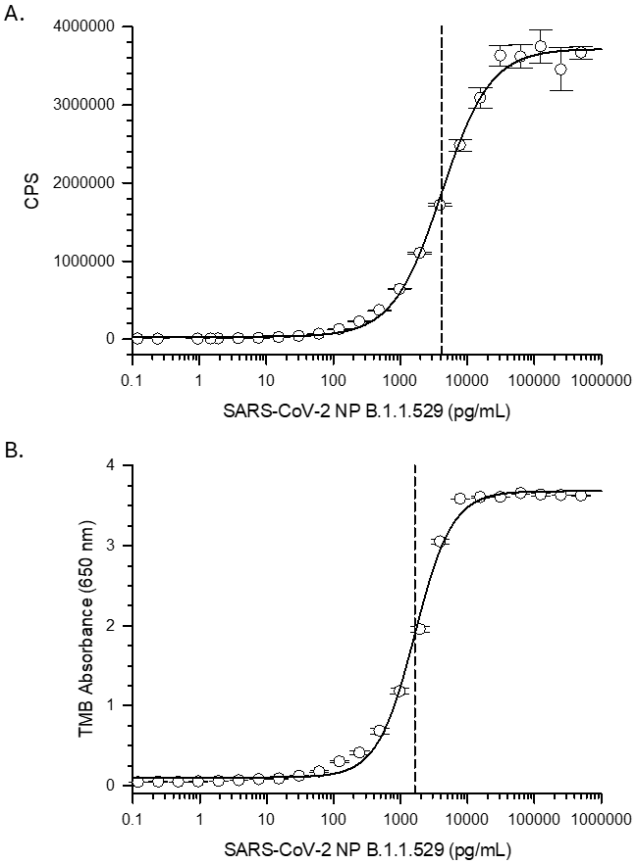

FIGURE 3 | Sandwich ELISA data plotting dose–response of 4D4 and 1H6-HRP binding to the SARS-CoV-2 Omicron B.1.1.529 NP variant. Chemiluminescent detection (panel A) is reported in counts per second (CPS) and colorimetric TMB detection in absorbance at 650 nm (panel B). Data points (open circles) represent the mean ± SEM. The solid line represents 4PL curve fit data and the vertical dashed line plots the assay EC50 value. Assay LODs are 15.3 pg/mL ($p = < 0.025$).

4 | Discussion

There remains concern regarding the persistence of the SARS-CoV-2 virus in various animal reservoirs and its evolutionary progression (Prince et al. 2021; Markov et al. 2023). Monitoring SARS-CoV-2 infection in wildlife and agriculturally important animal species remains a priority to limit the formation of animal reservoirs and reduce the risk of accelerated viral evolution in novel hosts and the emergence of SARS-CoV-2 viral variants of concern (VOC). Effective and affordable SARS-CoV-2 testing, especially in developing economies, is a cornerstone of ongoing global surveillance efforts. In this manuscript, we characterise the binding of two new SARS-CoV-2 NP MAbs (4D4 and 1H6) and describe their performance in sELISA and LFIA. The hybridoma cell lines making these MAbs represent transferable technology that de-risks critical intellectual property to facilitate the commercial availability of affordable SARS-CoV-2 tests.

The SARS-CoV-2 NP is a multi-domain, RNA-binding protein with an essential role in genome packaging and virion assembly (Zeng et al. 2020; Wu et al. 2023). Although the NP is packaged with RNA inside the assembled virus, it is found in abundance externally and has been demonstrated to be a useful antigenic target for detection of the virus and infected animals (Dutta et al. 2020; Lopez-Munoz et al. 2022). The NP structure is highly conserved across SARS-CoV-2 variants with a low rate of mutation to its primary structure (Lu et al. 2021; Zhang et al. 2021; Troyano-Hernaez et al. 2022; Yu et al. 2022). Its abundance during infection, antigenic availability, and stable primary structure is the basis for targeted MAb generation and the development of immunoassays with broad SAR-CoV-2 viral variant detection capability (Alhamid et al. 2022; Li et al. 2022; Yu et al. 2022; Song et al. 2023).

The evolution of the SARS-CoV-2 NP from the Wuhan Hu-1 to the Omicron B.1.1.529 variant resulted in a six amino acid change (P13L, ERS31-33 deletion, R203K, G204R); none of

TABLE 2 | Sandwich ELISA data reporting 4PL curve fit data for chemiluminescent (ECL) and 650 nm absorbance (TMB) of a recombinant a SARS-CoV-2 B.1.1.529 Omicron NP variant standard.

sELISA SARS-CoV-2 B.1.1.529 NP					
Substrate	**Instrument**	**Filter**	**Hillslope**	**EC50 (ng/mL)**	**LOD (pg/mL)**
ECL	Perkin-Elmer Victor X3	None	1.19	4.15	15.3 ($p = 0.014$)
TMB	Perkin-Elmer Victor X3	650 nm	1.55	1.63	15.3 ($p = 0.022$)

Note: Enhanced chemiluminescent substrate (ECL). 3,3′,5,5′ tetramethylbenzidine substrate (TMB). Pekin-Elmer Victor X3 is a multimode microplate reader. EC50 is half maximal effective concentration. LOD is limit of detection. Pairwise comparison against a no antigen control by Student's *t*-test reporting *p*-value.

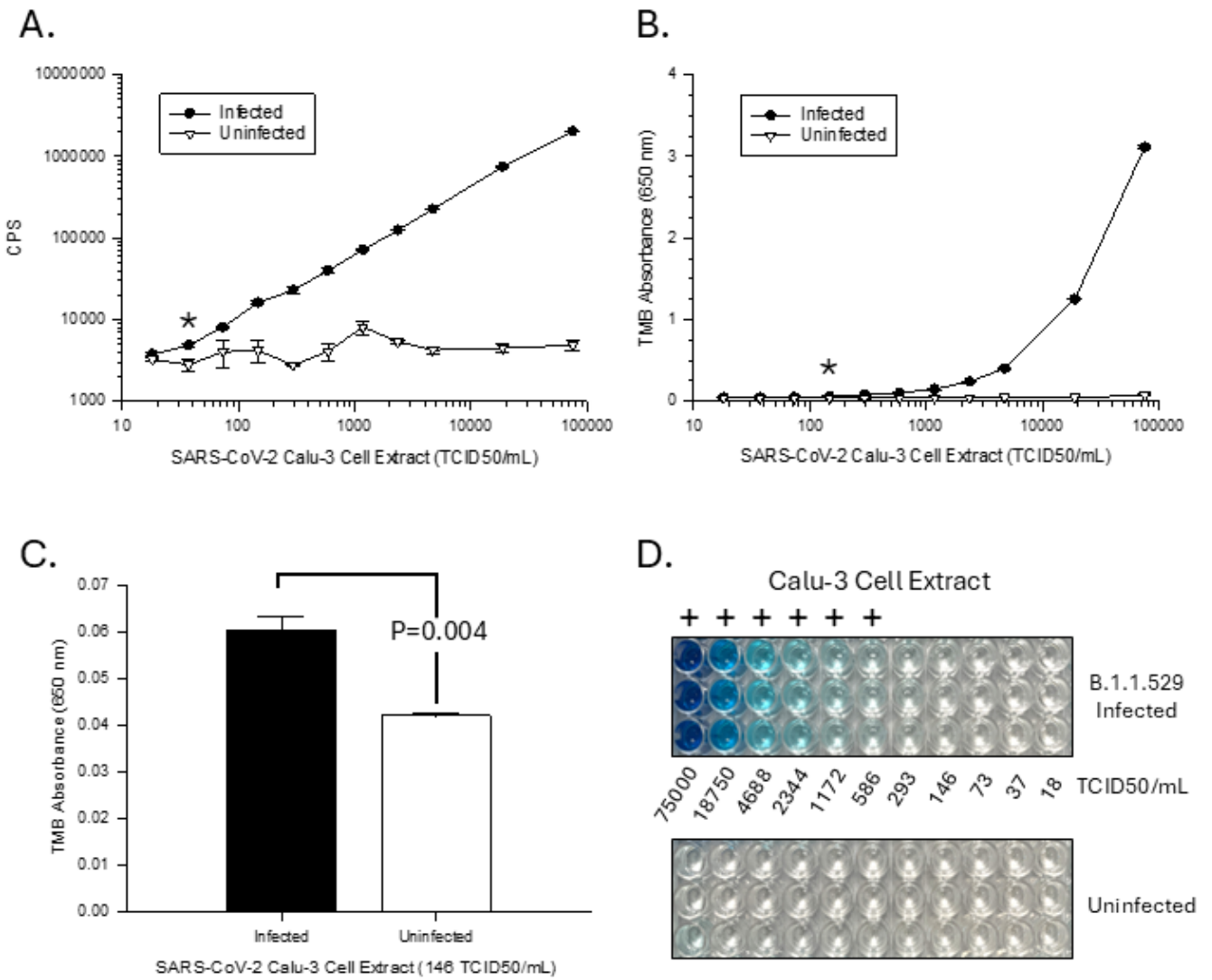

FIGURE 4 | Detection of the SARS-CoV-2 virus by sELISA. Serial dilutions of human Calu-3 cell extract infected with hCoV19/USA/GA-EHC-2811C/2021/Omicron B.1.1.529 virus (TCID50/mL = 1.5×10^6) were evaluated by chemiluminescent (panel A) and TMB (panel B–D) sELISA. Data plots the mean ± SEM (CPS or 650 nm absorbance) of viral infected extract (solid circle) or uninfected FBS control (open circle). The LOD of the chemiluminescent (panel A) and TMB assays (panel B, C) are 37 (*$p = 0.022$) and 146 TCID50/mL (*$p = 0.004$) respectively. A photograph of the blue TMB reaction product (panel D) visually reports (+) virus infected cell extract at 586 TCID50/mL. Viral genome equivalents per mL: 37 TCID50 = 1.44×10^5; 146 TCID50 = 5.67×10^5; 586 TCID50 = 2.28×10^6.

which impact our MAb binding by ELISA or Western blotting. Indeed, we see no significant differences in the binding of these MAbs to any of the SARS-CoV-2 NP variants evaluated, which includes BA.5 (data not shown), suggesting these immunoassays will detect all existing NP variants. We also see no difference in the binding of these MAbs to recombinant SARS-CoV-2 NP from *E. coli* or the glycosylated NP from HEK cells. Protein concentrations of hCoV NP were confirmed by spectroscopy and all had strong 280 nm peaks with a low 280/260 nm ratios (< 0.6), suggesting limited nucleotide binding to the recombinant proteins. In addition, we used terminal HIS-tag binding by dELISA (data not shown) to ensure adequate normalisation of protein given our negative MAb binding to other hCoV NP. The small differences in MAb binding to the SARS-CoV-2 NP variants is likely a function of protein normalisation estimates and distinct binding epitopes. Even with the high concentration of protein evaluated, 1 μg/mL by dELISA, 1 μg by Western blot, 2 μg/mL by LFIA (Figures 1–3C), MAb binding was limited to SARS-CoV-2 and SARS-CoV NPs. These NPs share 90.5% sequence identities, so binding of these MAbs to the biosimilar SARS-CoV NP is not overly surprising. However, we do observe a > 150-fold difference in 4D4 MAb binding to the SARS-CoV NP relative to SARS-CoV-2 by dELISA (Figure 1A). Moreover, the binding epitope of the 4D4 MAb to SARS-CoV NP is sensitive to heat denaturation, with no binding observed by Western blot (Figure 2A); suggesting conformational binding that is retained in the SARS-CoV-2, but not SARS-CoV NP. The use of the chaotrope guanidine hydrochloride (1 M Gdn-HCl for 1 h) to chemically disrupt protein structure (Hnasko et al. 2011) also resulted in a significant reduction (2.5-fold) in 4D4 MAb binding to SARS-CoV NP by dELISA (data not shown). Given the heat sensitivity of the 4D4 MAb binding epitope to the SARS-CoV NP, any sample heat treatment would likely make these immunoassays SARS-CoV-2 variant specific.

TABLE 3 | All hCoV viral samples were obtained as a courtesy from BEI Resources, NIAID, NIH, and the virus was passaged in cultured cells.

No.	SARS-Cov-2	Variant	Sample lot no.	Sample treatment	Sample ID	LOD genome copies/mL
1	USA-WA1	WA1	70039068	Irradiated	USA-WA1/2020 NR-52287	4.3×10^4 $p=0.005$
2	B.1.351	Beta	70045608	Heat	hCoV-19/USA/MD-HP01542/2021 NR-55350	8.6×10^4 $p=0.003$
3	B.1.351	Beta	70045298	Irradiated	hCoV-19/USA/MD-HP01542/2021 NR-55351	1.1×10^5 $p=<0.001$
4	B.1.351	Beta	70045299	Irradiated	hCoV-19/USA/MD-HP01542/2021 NR-55351	1.2×10^5 $p=<0.001$
5	B.1.617.2	Delta	70048021	Heat	hCoV-19/USA/MD-HP05285/2021 NR-56128	1.2×10^5 $p=0.036$
6	B.1.617.2	Delta	70048071	Irradiated	hCoV-19/USA/MD-HP05285/2021 NR-56128	3.8×10^5 $p=0.010$
7	B.1.1.529	Omicron	70050206	Heat	hCoV-19/USA/GA-EHC-2811C/2021 NR-56495	4.0×10^6 $p=<0.001$
8	B.1.1.529	Omicron	70050694	Irradiated	hCoV-19/USA/GA-EHC-2811C/2021 NR-56496	1.4×10^5 $p=0.022$
9	MERS-CoV	MERS	70003285	Irradiated	MERS-CoV EMC/2012 NR-50549	3.0×10^7 No Difference

Note: The viral genome copy number and TCID50 per mL were provided by the vendor. Cell culture media and lysates were gamma irradiated or heat denatured, and virus inactivation was confirmed. All samples were normalised by an initial dilution to a TCID50 of 1×10^4 and then serially diluted thereafter. Each dilution was evaluated by Student's t-test against a Vero E6 cell control, and *p*-values were reported with the calculated genome copies/mL at the limit of detection (LOD) from the chemiluminescent sELISA. No significant difference between MERS-CoV and Vero E6 control at any dilution was observed, and the table reports the genome copy number of the MERS-CoV diluted at the TCID50 of 1×10^4.

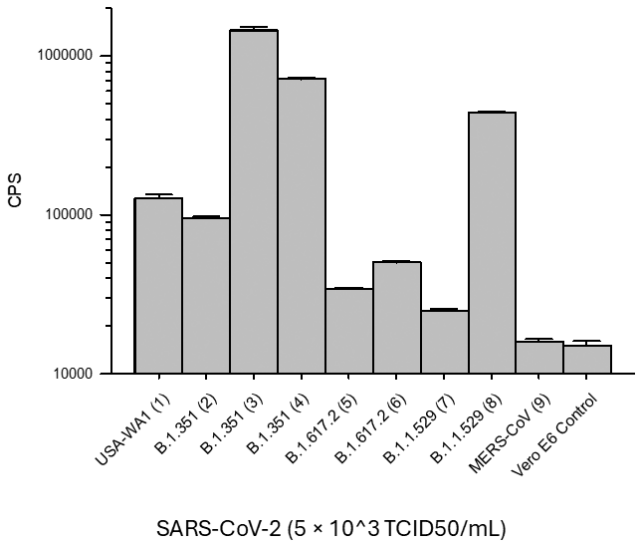

FIGURE 5 | Broad detection of SARS-CoV-2 viral variants by sELISA. Tissue culture passaged SARS-CoV-2 viral variants were inactivated by heat or gamma irradiation and evaluated by sELISA. See Table 3 (1–9) for sample details and LOD in viral genome equivalents/mL. All samples were normalised to 1×10^4 TCID50/mL then further diluted serially with chemiluminescent detection (CPS) by sELISA reported at 5×10^3 TCID50/mL. Data plots the mean ± SEM ($N=4$). At this TCID50 dilution all the SARS-CoV-2 variant samples were significantly different ($p=<0.001$) as compared to MER-CoV infected and an uninfected Vero E6 control (Student's *t*-test). No significant difference ($p=0.528$) was observed between MER-CoV infected and uninfected Vero E6 cell extracts.

Our microplate sELISA has a sensitivity of 15 pg/mL for the SARS-CoV-2 NP using chemistry suitable for detection with a luminometer or spectrophotometer. We report no impact of microplate drying after antibody immobilisation and blocking (> 6 mo 4°C desiccated) allowing reduced assay times (< 3 h). Colorimetric detection and the use of a spectrophotometer can be readily adapted to most laboratory settings at a low cost and have the added advantage of simple visual inspection of sample wells for reporting. The specificity of our sELISA for hCoV NP is limited to SARS-CoV-2 and SARS-CoV. Detection of SARS-CoV NP was significantly reduced compared to SARS-CoV-2 (> 2.5-log) with detection of 5 ng/mL ($p=0.006$) and 20 ng/mL ($p=0.001$) by the chemiluminescent and 650 absorbance assays respectively (data not shown). These sELSIAs exhibit a useful linear dynamic range, and a quantitative assessment of SARS-CoV-2 NP from samples could be determined from a standard curve (Table 2).

Importantly, we observed broad and sensitive detection of SARS-CoV-2 viral variants by sandwich immunoassays using the 4D4 and 1H6 MAb pair. In Figure 5 we show our chemiluminescent sELISA will broadly detect SARS-CoV-2 viral variants (USA-WA1, B.1.351, B.1.617.2 and B.1.1.529) with high sensitivity (Table 3). In Figure 4A,B, we plot a TCID50/mL dilution series of the SARS-CoV-2 B.1.1.529 viral variant and show detection by luminometry with a chemiluminescent substrate is ~4 times more sensitive than absorbance spectroscopy at 650 nm with a TMB substrate. However, the blue colour TMB reaction product provides visual reporting of viral detection (Figure 4D) and, like the LFIA, affords meaningful

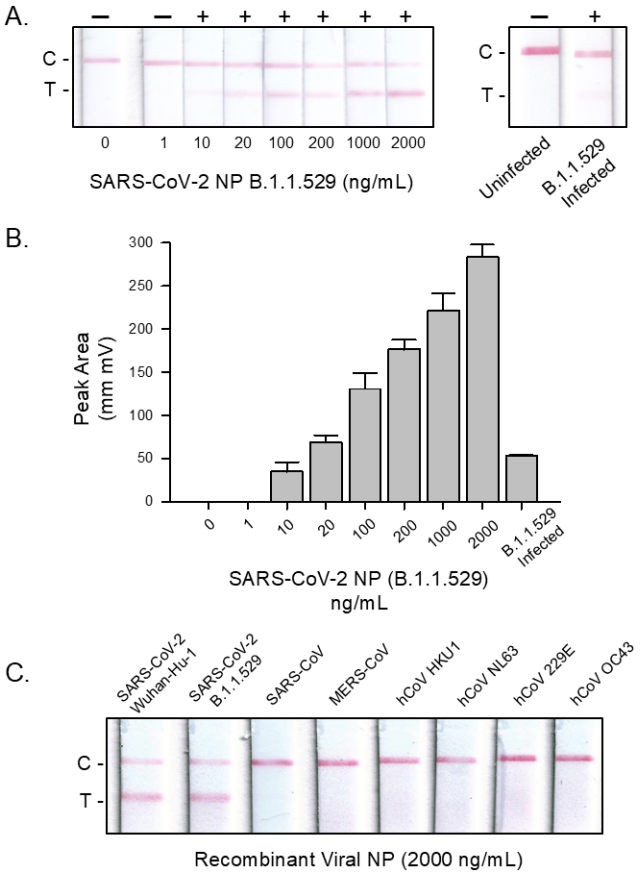

FIGURE 6 | Detection of SARS-CoV-2 by lateral flow immunoassay (LFIA) with a red particle (200 nm) reporter. A 10 ng/mL ($p = 0.037$) LOD of the LFIA was determined by evaluation of a SARS-CoV-2 NP (Omicron B.1.1.529 variant) dilution series at test line T (panel A, B). Human Calu-3 SARS-CoV-2 (B.1.1.529) infected cell extract (TCID50/mL 7.5×10^5) was positive at the test line (T) as compared to uninfected control ($p = < 0.001$). Recombinant viral nucleocapsid proteins (NP) were evaluated at 2 μg/mL by LFIA with positive test lines reported for the USA-WA-1 and Omicron B.1.1.529 SARS-CoV-2 NP variants with a faint test line visible for SARS-CoV NP (panel C). Reflectance at the test line (peak area mm mV) from samples run in triplicate are reported as mean ± SEM. Assay performance is confirmed by a positive control line (C).

detection thresholds without the need for instrumentation in a disposable and portable format suitable for pen-side detection. Although the LFIA provides visual results in < 10 min, it is at reduced sensitivity of SARS-CoV-2 NP (LOD = 10 ng/mL). No detection of hCoV NP by LFIA is reported, and it requires 2 μg/mL of SARS-CoV NP for a faint positive test line to resolve (Figure 6C).

In this manuscript, we developed and characterised immunoassays using a pair of novel MAbs (4D4 and 1H6) that bind the SARS-CoV and SARS-CoV-2 NP variants. We described their performance in microplate sELISA and LFIA and showed sensitive immunoassay detection of the SARS-CoV-2 virus from infected cells. Additional research should resolve putative MAb binding epitopes and determine if these MAbs have virus neutralising capability. Future optimisation of these immunoassays should be followed by field deployment to evaluate their detection capability of active viral variants in animal and environmental samples. The broad applicability of these MAbs across immunoassay platforms provides new opportunities for commercial test construction and resources that may augment existing SARS-CoV-2 detection technologies.

Author Contributions

Robert M. Hnasko: conceptualization, funding acquisition, writing – original draft, methodology, validation, visualization, writing – review and editing, formal analysis, supervision, resources, investigation, project administration, data curation. **Alice V. Lin:** investigation, methodology, validation, data curation, writing – review and editing. **Jeffery A. McGarvey:** writing – review and editing. **Eric S. Jackson:** methodology, validation, writing – review and editing.

Acknowledgements

The authors acknowledge funding from the U.S. Department of Agriculture (2030-32000-011-000-D; and 2030-32000-011-007-I).

Conflicts of Interest

The authors declare no conflicts of interest.

Data Availability Statement

The data that support the findings of this study are available from the corresponding author upon reasonable request.

References

Alhamid, G., H. Tombuloglu, A. A. Rabaan, and E. Al-Suhaimi. 2022. "SARS-CoV-2 Detection Methods: A Comprehensive Review." *Saudi Journal of Biological Sciences* 29: 103465.

Alwine, J. C., A. Casadevall, L. W. Enquist, F. D. Goodrum, and M. J. Imperiale. 2023. "A Critical Analysis of the Evidence for the SARS-CoV-2 Origin Hypotheses." *Journal of Virology* 97: e0036523.

Berche, P. 2023. "Gain-Of-Function and Origin of Covid19." *Presse Médicale* 52: 104167.

Blazquez-Fernandez, C., P. Lanza-Leon, L. Sanchez-Ruiz, and D. Cantarero-Prieto. 2023. "Economic Costs Related to Coronavirus Disease 2019 Pandemic: A Systematic Literature Review." *Science Progress* 106: 368504231201548.

Brown, C. 2004. "Emerging Zoonoses and Pathogens of Public Health Significance—An Overview." *Revue Scientifique et Technique* 23: 435–442.

Chen, C. L., C. C. Lai, D. L. Luh, et al. 2021. "Review of Epidemic, Containment Strategies, Clinical Management, and Economic Evaluation of COVID-19 Pandemic." *Journal of the Formosan Medical Association* 120, no. Suppl 1: S6–S18.

Ching, K. H., X. He, L. H. Stanker, A. V. Lin, J. A. McGarvey, and R. Hnasko. 2015. "Detection of Shiga Toxins by Lateral Flow Assay." *Toxins (Basel)* 7: 1163–1173.

Ching, K. H., A. Lin, J. A. McGarvey, L. H. Stanker, and R. Hnasko. 2012. "Rapid and Selective Detection of Botulinum Neurotoxin Serotype-A and -B With a Single Immunochromatographic Test Strip." *Journal of Immunological Methods* 380: 23–29.

Corman, V. M., D. Muth, D. Niemeyer, and C. Drosten. 2018. "Hosts and Sources of Endemic Human Coronaviruses." *Advances in Virus Research* 100: 163–188.

Cubuk, J., J. J. Alston, J. J. Incicco, et al. 2021. "The SARS-CoV-2 Nucleocapsid Protein Is Dynamic, Disordered, and Phase Separates With RNA." *Nature Communications* 12: 1936.

Dutta, N. K., K. Mazumdar, and J. T. Gordy. 2020. "The Nucleocapsid Protein of SARS-CoV-2: A Target for Vaccine Development." *Journal of Virology* 94: e00647-20.

Gostin, L. O., and G. K. Gronvall. 2023. "The Origins of Covid-19—Why It Matters (And Why It Doesn't)." *New England Journal of Medicine* 388: 2305–2308.

Hnasko, R., A. Lin, J. A. McGarvey, and L. H. Stanker. 2011. "A Rapid Method to Improve Protein Detection by Indirect ELISA." *Biochemical and Biophysical Research Communications* 410: 726–731.

Hnasko, R., A. V. Lin, and J. A. McGarvey. 2019. "Rapid Detection of Staphylococcal Enterotoxin-B by Lateral Flow Assay." *Monoclonal Antibodies in Immunodiagnosis and Immunotherapy* 38: 209–212.

Hnasko, R. M. 2015a. "The Biochemical Properties of Antibodies and Their Fragments." *Methods in Molecular Biology* 1318: 1–14.

Hnasko, R. M. 2015b. "Bioconjugation of Antibodies to Horseradish Peroxidase (HRP)." *Methods in Molecular Biology* 1318: 43–50.

Hnasko, R. M., E. S. Jackson, A. V. Lin, R. P. Haff, and J. A. McGarvey. 2021. "A Rapid and Sensitive Lateral Flow Immunoassay (LFIA) for the Detection of Gluten in Foods." *Food Chemistry* 355: 129514.

Hnasko, R. M., A. V. Lin, J. A. McGarvey, and C. P. Mattison. 2022. "Sensitive and Selective Detection of Peanut Allergen Ara h 1 by ELISA and Lateral Flow Immunoassay." *Food Chemistry* 396: 133657.

Hnasko, R. M., and J. A. McGarvey. 2015. "Affinity Purification of Antibodies." *Methods in Molecular Biology* 1318: 29–41.

Hnasko, R. M., and L. H. Stanker. 2015. "Hybridoma Technology." *Methods in Molecular Biology* 1318: 15–28.

Hnasko, T. S., and R. M. Hnasko. 2015. "The Western Blot." *Methods in Molecular Biology* 1318: 87–96.

Holmes, E. C., S. A. Goldstein, A. L. Rasmussen, et al. 2021. "The Origins of SARS-CoV-2: A Critical Review." *Cell* 184: 4848–4856.

Li, X., M. Xiong, Q. Deng, X. Guo, and Y. Li. 2022. "The Utility of SARS-CoV-2 Nucleocapsid Protein in Laboratory Diagnosis." *Journal of Clinical Laboratory Analysis* 36: e24534.

Lopez-Munoz, A. D., I. Kosik, J. Holly, and J. W. Yewdell. 2022. "Cell Surface SARS-CoV-2 Nucleocapsid Protein Modulates Innate and Adaptive Immunity." *Science Advances* 8: eabp9770.

Lu, S., Q. Ye, D. Singh, et al. 2021. "The SARS-CoV-2 Nucleocapsid Phosphoprotein Forms Mutually Exclusive Condensates With RNA and the Membrane-Associated M Protein." *Nature Communications* 12: 502.

Markov, P. V., M. Ghafari, M. Beer, et al. 2023. "The Evolution of SARS-CoV-2." *Nature Reviews. Microbiology* 21: 361–379.

Masters, P. S. 2006. "The Molecular Biology of Coronaviruses." *Advances in Virus Research* 66: 193–292.

Masters, P. S., L. Kuo, R. Ye, K. R. Hurst, C. A. Koetzner, and B. Hsue. 2006. "Genetic and Molecular Biological Analysis of Protein-Protein Interactions in Coronavirus Assembly." *Advances in Experimental Medicine and Biology* 581: 163–173.

Mohammed, M. E. A. 2021. "The Percentages of SARS-CoV-2 Protein Similarity and Identity With SARS-CoV and BatCoV RaTG13 Proteins Can Be Used as Indicators of Virus Origin." *Journal of Proteins and Proteomics* 12: 81–91.

Prince, T., S. L. Smith, A. D. Radford, T. Solomon, G. L. Hughes, and E. I. Patterson. 2021. "SARS-CoV-2 Infections in Animals: Reservoirs for Reverse Zoonosis and Models for Study." *Viruses* 13: 494.

Richards, F., P. Kodjamanova, X. Chen, et al. 2022. "Economic Burden of COVID-19: A Systematic Review." *ClinicoEconomics and Outcomes Research* 14: 293–307.

Sakamoto, S., W. Putalun, S. Vimolmangkang, et al. 2018. "Enzyme-Linked Immunosorbent Assay for the Quantitative/Qualitative Analysis of Plant Secondary Metabolites." *Journal of Natural Medicines* 72: 32–42.

Sanchez, C. A., J. Venkatachalam-Vaz, and J. M. Drake. 2021. "Spillover of Zoonotic Pathogens: A Review of Reviews." *Zoonoses and Public Health* 68: 563–577.

Scobey, T., B. L. Yount, A. C. Sims, et al. 2013. "Reverse Genetics With a Full-Length Infectious cDNA of the Middle East Respiratory Syndrome Coronavirus." *Proceedings of the National Academy of Sciences of the United States of America* 110: 16157–16162.

Shen, J., Y. Li, H. Gu, F. Xia, and X. Zuo. 2014. "Recent Development of Sandwich Assay Based on the Nanobiotechnologies for Proteins, Nucleic Acids, Small Molecules, and Ions." *Chemical Reviews* 114: 7631–7677.

Song, W., Z. Fang, F. Ma, et al. 2023. "The Role of SARS-CoV-2 N Protein in Diagnosis and Vaccination in the Context of Emerging Variants: Present Status and Prospects." *Frontiers in Microbiology* 14: 1217567.

Stanker, L. H., and R. M. Hnasko. 2015. "A Double-Sandwich ELISA for Identification of Monoclonal Antibodies Suitable for Sandwich Immunoassays." *Methods in Molecular Biology* 1318: 69–78.

Tan, C. C. S., S. D. Lam, D. Richard, et al. 2022. "Transmission of SARS-CoV-2 From Humans to Animals and Potential Host Adaptation." *Nature Communications* 13: 2988.

Tang, G., Z. Liu, and D. Chen. 2022. "Human Coronaviruses: Origin, Host and Receptor." *Journal of Clinical Virology* 155: 105246.

Troyano-Hernaez, P., R. Reinosa, and A. Holguin. 2022. "Evolution of SARS-CoV-2 in Spain During the First Two Years of the Pandemic: Circulating Variants, Amino Acid Conservation, and Genetic Variability in Structural, Non-Structural, and Accessory Proteins." *International Journal of Molecular Sciences* 23: 6394.

Wu, W., Y. Cheng, H. Zhou, C. Sun, and S. Zhang. 2023. "The SARS-CoV-2 Nucleocapsid Protein: Its Role in the Viral Life Cycle, Structure and Functions, and Use as a Potential Target in the Development of Vaccines and Diagnostics." *Virology Journal* 20: 6.

Yount, B., K. M. Curtis, and R. S. Baric. 2000. "Strategy for Systematic Assembly of Large RNA and DNA Genomes: Transmissible Gastroenteritis Virus Model." *Journal of Virology* 74: 10600–10611.

Yount, B., K. M. Curtis, E. A. Fritz, et al. 2003. "Reverse Genetics With a Full-Length Infectious cDNA of Severe Acute Respiratory Syndrome Coronavirus." *Proceedings of the National Academy of Sciences of the United States of America* 100: 12995–13000.

Yu, J., Z. Qin, X. Liu, et al. 2022. "High-Specificity Targets in SARS-CoV-2 N Protein for Serological Detection and Distinction From SARS-CoV." *Computers in Biology and Medicine* 143: 105272.

Zeng, L. P., Y. T. Gao, X. Y. Ge, et al. 2016. "Bat Severe Acute Respiratory Syndrome-Like Coronavirus WIV1 Encodes an Extra Accessory Protein, ORFX, Involved in Modulation of the Host Immune Response." *Journal of Virology* 90: 6573–6582.

Zeng, W., G. Liu, H. Ma, et al. 2020. "Biochemical Characterization of SARS-CoV-2 Nucleocapsid Protein." *Biochemical and Biophysical Research Communications* 527: 618–623.

Zhang, Y., C. M. Ong, C. Yun, et al. 2021. "Diagnostic Value of Nucleocapsid Protein in Blood for SARS-CoV-2 Infection." *Clinical Chemistry* 68: 240–248.

Supporting Information

Additional supporting information can be found online in the Supporting Information section.